Field-induced directional surface anisotropy in an NiMn alloy

1993 J. Phys.: Condens. Matter 5 5443

(http://iopscience.iop.org/0953-8984/5/31/009)

J. Phys.: Condens. Matter 5 (1993) 5443–5458. Printed in the UK

Field-induced directional surface anisotropy in an NiMn alloy

B Aktas† and Y Oner‡

† Department of Physics, University of California, San Diego, California 92093, USA
‡ Department of Physics Engineering, Hacettepe University, Beytepe, Ankara, Turkey

Received 15 March 1993, in final form 19 May 1993

Abstract. Magnetic properties of the reentrant $Ni_{76}Mn_{24}$ alloy have been studied as a function of temperature by using both ferromagnetic resonance (FMR) and DC magnetization techniques. The experiments were performed either by applying the DC field after cooling the sample to 4 K (ZFC case) or by cooling the sample in the presence of an external field (FC case). In the FC case, the field-induced unidirectional anisotropy field acting on the surface spins is much stronger than that acting on the inner spins, probably due to the lower symmetry of the structure at the surface. This effect causes surface-induced modes to appear in addition to usual FMR bulk mode, when the measuring field is applied opposite to the field in which the sample is cooled. Introducing a unidirectional surface anisotropy energy into the (Rado and Weertman) general exchange boundary conditions, we analysed the experimental data and obtained magnetic parameters such as the surface-induced exchange anisotropy, bulk anisotropy and exchange stiffness constant as a function of temperature. A strong correlation has been observed between the field-induced exchange anisotropy deduced from FMR and the hysteresis effect observed in DC magnetization data.

1. Introduction

Considerable attention has recently been given to alloys with exchange anisotropy mainly because of the unusual behaviour of a number of their physical properties. The NiMn system is a typical example in which the static and the dynamic magnetization exhibit unusual behaviour (i.e., a displaced hysteresis loop upon cooling in a field, the abrupt rise of the non-equilibrium magnetization with increasing temperature below T_f where strong magnetic irreversibility sets in, and the frequency dependence of T_f). None of these are well understood on a bulk level. For Mn concentrations below 24 at%, the system exhibits a spin glass (SG)-like state at the lowest temperature, a paramagnetic (PM) state at the highest temperature and a state with ferromagnetic (FM)-like properties at intermediate temperatures. Above 24 at% Mn, however, the NiMn system goes from a PM state to an SG phase with decreasing temperature.

Recently, the authors [1, 2] have interpreted their ferromagnetic resonance (FMR) data for NiMn alloys in terms of the domain anisotropy model which was proposed on the basis of resistivity [3] as well as magnetization studies [4, 5]. According to this model, the sample is composed of a large number of randomly oriented small domains where each domain has a unidirectional anisotropy, H_A, directed along the initial direction of the saturated magnetization vector M_s. It was also claimed [1, 2, 5] that the unidirectional anisotropy is not rigidly linked to the lattice along its initial direction, but can be rotated elastically by the applied magnetic field. This assertion has been supported by the perpendicular AC susceptibility measurements made on $Ni_{77}Mn_{23}$ samples [6].

0953-8984/93/315443+16$07.50

A recent study [7] on thin films of NiMn alloys shows that the unidirectional anisotropy is smaller than in bulk specimens and is also highly unstable against the cycling of a few kG applied field at 4.2 K. Abdul-Razzaq [8] also found that the unidirectional anisotropy of $Ni_{74}Mn_{26}$ decreases with the decreasing film thickness. This leads us to consider that the unidirectional anisotropy on the layers near the surface could differ from that in the body of a bulk specimen and this difference would manifest itself in the FMR spectra.

On the other hand, Teale and Pelegrini [9] have clearly identified and theoretically justified the presence in the observed resonance spectra of single-crystal specimens of $GdAl_2$, of an exchange-dominated surface mode arising from a specific magnitude and symmetry of the pinning of the transverse microwave magnetization at the surface of the bulk specimen. In their case, this pinning is essentially due to surface-induced magnetocrystalline anisotropy forces. In fact, such surface modes have been observed in ferromagnetic thin films and theoretically described in the papers by Puszkarski [10] and Rado *et al* [11, 12]. Our aim in this work is to investigate the effects of field-induced directional anisotropy on the FMR spectra in the disordered $Ni_{76}Mn_{24}$ alloy.

2. Theoretical framework

The power absorbed by the sample in a microwave cavity, and hence the integral of our measured resonance signals, is proportional to the real part of the surface impedance. The general procedure for the calculation of Z was given in the literature [9] for the sample geometries illustrated in figure 1. Using field-induced anisotropies and Bloch-type damping instead of Landau–Lifshitz damping, we adapted their results to the surface impedance.

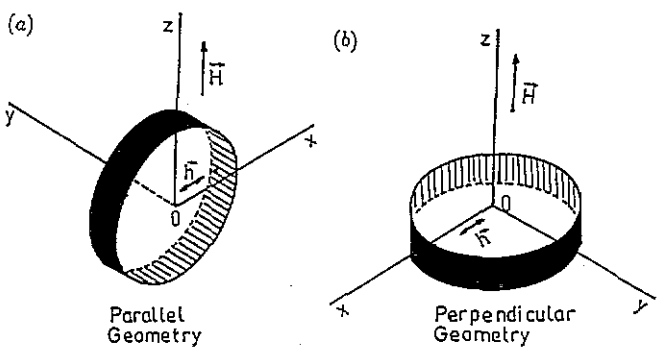

Figure 1. Geometries used to calculate the response to microwave radiation incident on a bulk ferromagnet.

2.1. Parallel geometry

The high-frequency complex surface impedance Z' for the parallel geometry in figure 1 is given by

$$Z' = \frac{Q_1(B_2A_3 - B_3A_2) + Q_2(B_3A_1 - B_1A_3) + Q_3(B_1A_2 - B_2A_1)}{(B_2A_3 - B_3A_2) + (B_3A_1 - B_1A_3) + (B_1A_2 - B_2A_1)} \qquad (1)$$

where

$$A_n = (Q_n^2 - 2i\epsilon^2)(Q_n + \xi_x^{n,r})/(i8\pi\epsilon^2)$$
$$B_n = i\Omega(Q_n^2 - 2i\epsilon^2)(Q_n + \xi_y^{n,r})/(i8\pi\epsilon^2)(1 + \eta - Q_n^2). \tag{2}$$

Here, the Q_ns are related spin-wave vectors q_n

$$Q_n^2 = q_n^2 A/2\pi M_z^2$$

and consist of three positive roots for

$$Q^6 - C_1 Q^4 + C_2 Q^2 - C_3 = 0 \tag{3}$$

where

$$C_1 = 1 + 2\eta + 2\epsilon^2 i$$
$$C_2 = \eta(\eta + 1) - \Omega^2 + 4\epsilon^2 i(1 + \eta)$$
$$C_3 = 2\epsilon^2 i((1 + \eta)^2 - \Omega^2) \tag{4}$$

with

$$\eta = H_z^{\text{eff}}/4\pi M_z$$
$$\Omega = (\omega - i/T_2)/\gamma 4\pi M_z$$
$$\epsilon^2 = 4\pi \times 10^{-3} \times A\gamma\Omega/M_z\rho. \tag{5}$$

Here H_z^{eff} is the effective field which consists of the applied field, the demagnetizing field and the total anisotropy field. T_2 is the relaxation time of the transverse component of magnetization, ω is the microwave frequency, γ is the gyromagnetic ratio, A is the effective exchange constant, and $\rho(= 1/\sigma)$ is the electrical resistivity in $\mu\Omega$ cm. It should be noted that M_z is the magnetization of the specimen where the resonance occurs while M_s is the saturation magnetization. For a reentrant polycrystalline sample, the only possible magnetic anisotropy is the field-induced unidirectional anisotropy. We assume the following expression

$$H_{\text{ani}} = [(K_1 + K_2)/M_z]i_z \tag{6}$$

for the bulk anisotropy field where K_1 and K_2 represent the rigid and dynamic components of the unidirectional field-induced bulk anisotropy energy respectively, and i_z is the unit vector along the applied DC field direction. Since K_1 represents the rigid component of the anisotropy field, its sign is positive when the measuring field is along the cooling field direction and negative for the reverse field direction. In (2) $\xi_x^{n,r}$ and $\xi_y^{n,r}$ are surface spin pinning parameters and should be deduced from an appropriate surface anisotropy energy. The surfaces of magnetic thin films are taken into account by introducing a phenomenological uniaxial surface anisotropy energy given by [12]

$$E_{\text{surf}} = -k_s \cos^2\theta \tag{7}$$

where θ is the angle between the magnetization and the symmetry axis which is chosen normal to the film surface. Negative values of k_s correspond to an easy-plane anisotropy with a hard-axis normal to the film surface, and positive values correspond to an easy-axis along the normal direction. In this study, however, we introduce first the unidirectional component to the surface energy density and take it as the sum of directional and axial term which lead to the surface field

$$H_{\text{surf}} = (2k_2/M_z)u_y i_n + (k_1/M_z)i_z \tag{8}$$

where k_1 represents the unidirectional surface anisotropy along the cooling field direction i_z and k_2 represents the uniaxial surface-induced anisotropy fields along the direction i_n normal to the sample surface. Using these surface anisotropy fields and following the procedure in [9] we obtain

$$\xi_x^{n,r} = \mp(8\pi A)^{-1/2}H_a \qquad \xi_y^{n,r} = -(8\pi A)^{-1/2}(H_k \pm H_a) \tag{9}$$

where $H_a = +k_1/M_s$ and $H_k = 2k_2/M_s$. Note that $n(r)$ corresponds to the case in which the applied field is directed along (opposite) the cooling field direction. The lower (upper) sign corresponds to the n case (r case).

2.2. *Perpendicular geometry*

The surface impedance for perpendicular geometry is calculated in a similar fashion to [9]. Maxwell's equations and the Landau–Lifshitz equation of motion for magnetization are written in component form and combined to give a secular equation for the propagation constants of the microwave field in the form

$$Q^4 - D_{\mp 1}Q^2 + D_{\mp 2} = 0 \tag{10}$$

where

$$D_{\mp 1} = \eta + 2\epsilon^2 \mathrm{i} \mp \Omega \qquad D_{\mp 2} = 2\epsilon^2(1+\eta)\mathrm{i} \mp 2\epsilon^2\Omega.$$

Thus, we find two biquadratic equations, where + (−) signs correspond to right (left) polarization of the RF electromagnetic field. For this case the surface boundary conditions yield the following expression for surface impedance

$$Z' = (Z'_+ + Z'_-)/2 \tag{11}$$

where

$$Z'_{\mp} = (A_{\mp 1}Q_{\mp 2} - A_{\mp 2}Q_{\mp 1})/(A_{\mp 2} - A_{\mp 1})$$

$$A_{\mp n} = (Q^2_{\mp n} - 2\mathrm{i}\epsilon^2)(Q_{\mp n} + \xi^{n,r}_{x,y})$$

$$\xi^{n,r}_{x,y} = \xi^{n,r}_x = \xi^{n,r}_y = (8\pi A)^{-1/2}(H_k \pm H_a).$$

Here, the + (−) signs in $\xi_{x,y}$ correspond to the $n(r)$ case and $H_k = 2k_2/M_z$, $H_a = k_1/M_z$.

3. Results and discussion

Samples in sealed quartz tubes at 0.3 atm Ar pressure were melted twice using an inductance furnace to ensure better homogeneity. Cold working was employed to roll the alloy into a sheet from which an experimental sample of 250 μm thickness and 3 mm diameter was cut. Finally, the sample was annealed at 850 °C for 1 h in a quartz tube under vacuum, quenched by allowing high-pressure Ar gas into the tube and then dropping the sample into cold water. This treatment is performed in order to achieve the best disordered state. However, it is almost impossible to avoid a small amount of short-range order (Ni_3Mn clusters), especially near the multicritical point (24.5 at% Mn in Ni). AC susceptibility measurements on the same sample [5] show a Curie temperature of about 240 K and a sharp drop in the susceptibility indicating that the freezing temperature is at about 115 K. Resistivity measurements have also been carried out on the same sample and $\rho\,(T = 4.2\ \mathrm{K}) = 55\ \mu\Omega$ cm is in good agreement with a previous study [19].

The magnetization was measured with a home-made magnetometer for temperatures varying from 4 to 300 K and under applied fields up to 23 kG. FMR measurements were performed with a Varian Associates reflection spectrometer at a fixed frequency (9.25 GHz). For both experiments, we have used the same cryostat (an Oxford Helium Flow Cryostat). Further experimental details have been given in a previous work [2]. We have taken the spectra under various experimental conditions. In some experiments, the sample was cooled in a magnetic field H_{cool} through the freezing temperature (field cooling, FC case), then the spectra were taken in a magnetic field applied along the direction of H_{cool} (normal FC or n-FC case) and the spectra were recorded again by reversing the applied magnetic field (to be referred to as the r-FC case). Similarly, ZFC represents the case in which the spectra were recorded immediately after cooling the sample in zero field. Furthermore, both the magnetization and the spectra were stored in digital form using a microcomputer for both parallel and perpendicular geometries after the sample initially was cooled to 4.2 K and then warmed up to various fixed measurement temperatures up to 300 K.

The calculation of $\mathrm{d}(\mathrm{Re}(Z))/\mathrm{d}H_0$ as a function of H_0 was performed on a prime computer. Model programs displayed the computed curve on a visual display unit where the measured curves could also be plotted for comparison. The program could be used interactively and the operator would adjust the parameters to obtain an eye-fit between theory and experiment.

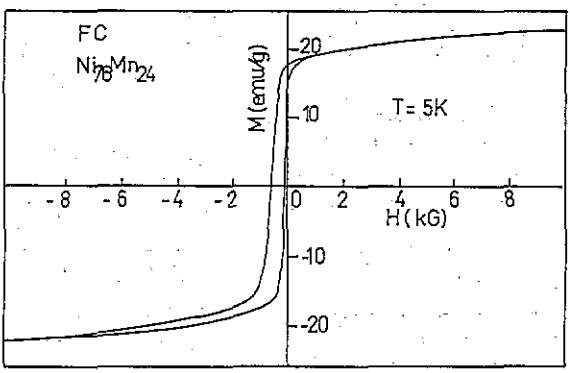

Figure 2. The hysteresis loop for $Ni_{76}Mn_{24}$ recorded after cooling the sample in a field of 10 kG down to 5 K (indicated by FC).

Figure 2 shows a complete hysteresis cycle at 5 K for $Ni_{76}Mn_{24}$. A recorded hysteresis loop was started at the cooling field of 10 kG; the field was then swept to −10 kG and back again to 10 kG which is similar to a field sweep in conventional FMR measurements. The domain magnetization $M_s(= 24$ emu $g^{-1})$ is taken to be the average value at positive $H(= +10$ kG) and negative $H(= -10$ kG). As seen from the figure, the hysteresis loop is shifted to the negative field side by about 280 G. The average coercive field is 200 G. A selection of the hysteresis loops for ZFC cases are presented in figure 3. It is clear from the figures that the FMR resonance occurs at fields where the magnetization does not reach yet its saturation value. Therefore magnetization data as a function of applied field were taken to calculate the FMR spectra for a given temperature. At temperatures lower compared to the freezing temperature, the anisotropy parameters K_1 can be deduced from the hysteresis loops; the shift of the centre of the loops H_A is taken to be K_1/M_s.

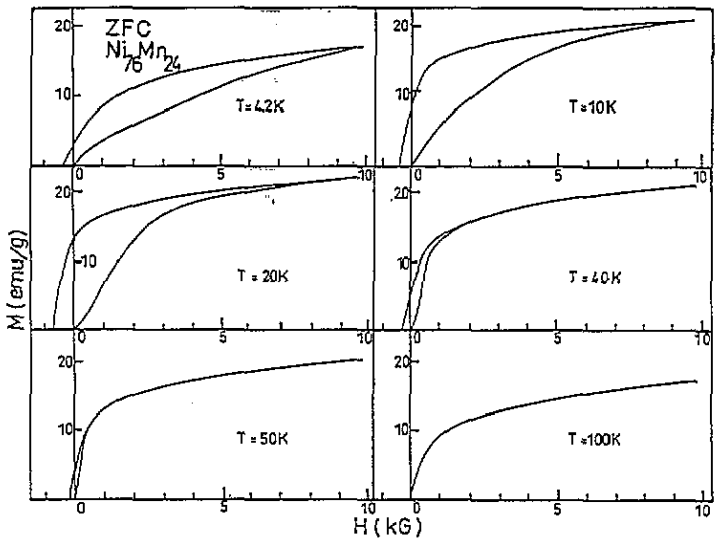

Figure 3. A set of hysteresis loops for $Ni_{76}Mn_{24}$ cooled in zero field (ZFC) down to the temperatures of measurements indicated on the figure. Note that the lower branches belong to the initial magnetization.

Figures 4, 5 and 6 show the experimental values of differential resonance absorption of $Ni_{76}Mn_{24}$ as a function of the applied field, together with the theoretical curves at some selected temperatures for both FC and ZFC cases. As can be seen in figure 4, the spectra for the *r*-FC case, especially at $T = 7$ K, exhibit clearly two resolved resonance lines while for *n*-FC cases, these two resonance lines overlap and give a single asymmetric line. That is, the relatively weak resonance line at higher field disturbs the high-field side of the main resonance at lower fields and gives such a single asymmetric line. Double peaks for some bulk ferromagnetic samples have also been observed by several authors [9] who pointed out that the secondary mode appeared due to the existence of surface uniaxial anisotropy. Teale and Pelegrini [9] concluded that the surface mode is shifted from the bulk mode to higher fields with increasing positive values of the surface anisotropy constant corresponding to an easy-axis normal to the sample surface. The intensity ratio of the surface-induced mode to the bulk mode increases with the magnetic stiffness constant A. It is obvious that the

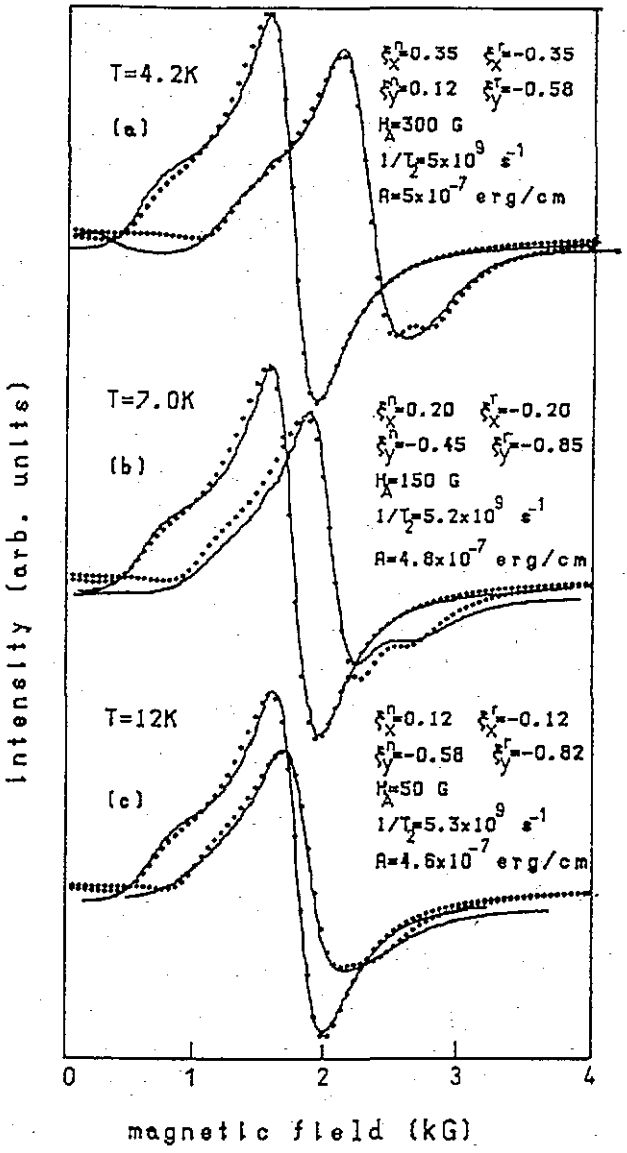

Figure 4. Measured (full curves) and calculated FMR spectra for parallel geometry of $Ni_{76}Mn_{24}$ alloy recorded as a function of applied magnetic field for *n*-FC (left-hand side) and *r*-FC (right-hand side) cases at (*a*) 4.2 K (*b*) 7 K and (*c*) 12 K. The parameters ξ_x, ξ_y, $1/T_2$, A indicated on the figure were deduced from a theoretical fit of the resonance curves to the corresponding experimental ones. The values of H_A were obtained from the differences of the resonant fields for *n*-FC and *r*-FC cases.

distance from the bulk mode to the surface mode must be symmetric with respect to the positive and negative field directions. However, this symmetry is broken in our spectra as shown in figure 4. As observed, the surface mode in *r*-FC cases is shifted to much higher fields than that in *n*-FC cases. This shift in *n*-FC cases is so small that it is difficult to identify. This asymmetric behaviour of our experimental spectra, therefore, leads us to suggest that

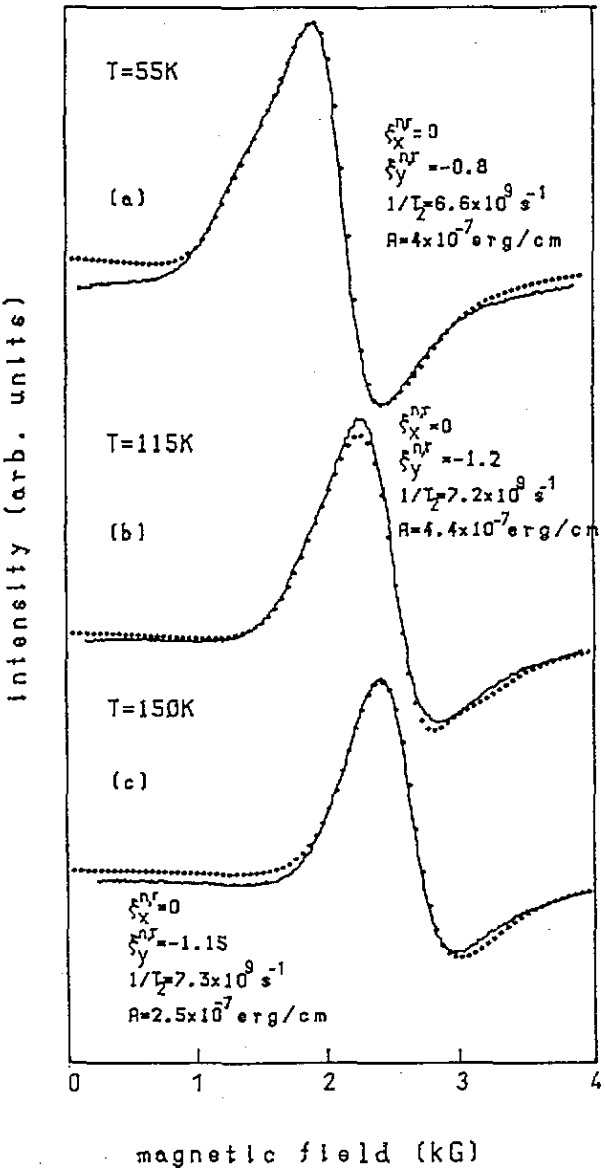

Figure 5. Measured (full curves) and calculated FMR spectra as a function of applied magnetic field at some selected temperatures $T > T_M = 30$ K, where the unidirectional anisotropy vanishes, for a parallel geometry of $Ni_{76}Mn_{24}$. The fitting parameters (ξ_x, ξ_y, $1/T_2$, A) are indicated on the figure for each T.

the surface anisotropy should include a directional component, the unidirectional term.

Taking into account the directional component of the surface anisotropy, theoretical curves were computed by evaluating the surface impedance formula (1) and (11). In order to fit the theoretical curves to experimental ones, the following methods have been employed.

The experimental curves correspond to the field derivative of the real component of the surface impedance, given by (1) and (11). There are nine parameters to be determined; namely, the magnetization M_z, the gyromagnetic ratio, the rigid and dynamic

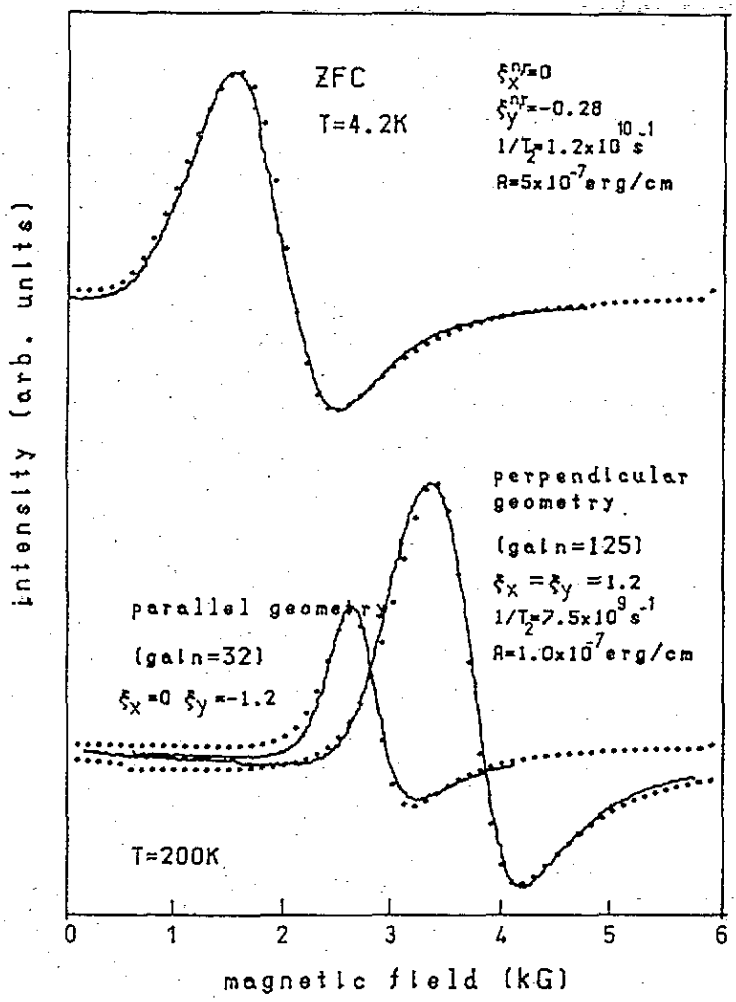

Figure 6. Measured (full curves) and calculated FMR spectra at $T = 4.2$ K for the parallel geometry of $Ni_{76}Mn_{24}$ alloy for the ZFC case (upper) and the lower shows the FMR spectra for both parallel and perpendicular geometries at $T = 200$ K. Note that the receiver gains for parallel and perpendicular geometries are different at $T = 200$ K, as indicated on the figure.

components of the unidirectional anisotropy $H_A(= K_1/M_z)$ and $H_K(= 2K_2/M_z)$, the exchange stiffness constant A, the resistivity ρ, the damping parameters $1/T_2$, and the surface anisotropy parameters k_1 and k_2. The magnetization values have been taken from the static magnetization measurements made on the same sample. In order to eliminate the uncertainty in magnetization, we have also measured the magnetization simultaneously with FMR by measuring the shift of a single DPPH marker (diphenyl pierylhydrazyl) located on the surface of the sample and compared it to another one sufficiently far away from the sample. Since the difference in their resonance fields is proportional to the magnetization, we could obtain additional information about the relative change of magnetization with temperature. The resistivity values have also been used [20] from the data taken on a sample cut from the same $Ni_{76}Mn_{24}$ button. These values vary between 55 and 65 $\mu\Omega$ cm in the temperature range 4–200 K. Fitting the data obtained in parallel and perpendicular

geometries at temperatures where $H_A = 0$ and $H_K = 0$, leads to the absolute value of magnetization and a nearly temperature-independent γ value, corresponding to $g = 2.16$ for all temperatures. The differences in the resonance fields, which correspond to the rigid component of anisotropy ($= 2H_A$), observed in n-FC and r-FC cases in FMR spectra are twice as large as the hysteresis shift. It should be noted that, at very low temperatures the system is so rigid magnetically that there is fairly good agreement between the rigid component of the unidirectional anisotropy fields determined from the hysteresis loop measurements and from the FMR data. However, as the temperature increases the lifetime of the DM anisotropy becomes smaller and smaller and it can no longer be deduced from DC magnetization. However, if one considers the characteristic time of ESR (10^{-10} s), it is still sufficiently long lived to be detected in FMR measurements [21]. Therefore, at higher temperatures the anisotropy parameters K_1 and K_2 were deduced from FMR data while at low temperatures, K_1 at least can be obtained either from DC magnetization [13, 14] or FMR data. The total rigid shift of the resonance field from the line calculated by using only the M and g values corresponds to the total anisotropy fields ($= H_A + H_K$). Thus, the remaining four parameters A, $1/T_2$, k_1 and k_2 can be adjusted so as to obtain a good agreement between the line shapes of the calculated and the experimental spectra.

Two resonance lines occur only for sufficiently negative values of either ξ_x or ξ_y. The separation of the two resonances increases as these parameters become more and more negative. While the higher-field mode shifts to higher fields due to magnetic surface anisotropy, the absorption line at lower fields is essentially unshifted. In addition, the effect of ξ_x on the shift for parallel geometry is greater than that of ξ_y. While ξ_y includes the difference between the unidirectional and the uniaxial components, ξ_x depends only on the directional anisotropy. This explains why the separation of the two resonance lines depends on the positive and negative field directions.

A closer examination shows that a shoulder appears in the low-field side of the resonance curves as shown in figure 4. Hurdequint *et al* [22] have also mentioned the presence of a shoulder in their experiments on $Ni_{74}Mn_{26}$. The position of this kink depends strictly on the magnetization and approaches the main resonance line as the magnetization M decreases, consistently with the calculated curves. Hence, at higher temperatures, this kink significantly modifies the low-field side of the resonance curves as can be seen in figures 5 and 6.

The spectra for n-FC and r-FC cases coincide with each other at $T_M = 30$ K where the rigid component of the unidirectional anisotropy vanishes. Increasing the temperature further, the spectra for FC and ZFC cases becomes almost identical in every respect (such as lineshape, field for resonance, linewidth, amplitude etc.). However, at low temperatures, the spectra for ZFC cases are much broader and weaker in amplitude although the values of the resonance fields are comparable in magnitude. Furthermore, the extra linewidth in the ZFC case is concomitant with the presence of a randomly distributed rigid unidirectional anisotropy field H_A induced along the direction of each individual domain magnetization (see figure 6 of [2]). That is, each domain experiences a different effective field and therefore, the precision of M dephases from domain to domain. Consequently a gradient in the transverse component of average magnetization M (local spin waves) are induced in the sample. These spin-wave modes have also been observed in $Ni_{79}Mn_{21}$ alloys by inelastic neutron diffraction studies [23]. Briefly, at lower temperatures, the absorption lines also comprise many spin-wave modes for ZFC case. As a result, the extra linewidth compared with FC case can be attributed to these inhomogeneous magnetic domain anistropy fields. As can be seen in figure 7, linewidth curves for both FC and ZFC cases join together at $T_M = 30$ K, then increase smoothly up to the freezing temperature $T_f = 115$ K and level off at higher temperatures. Note that this behaviour is qualitatively similar to that observed

in [24]. This is likely to be due to the extra contribution to the exchange narrowing process due to the increasing local DM anisotropy [21] as the temperature decreases. In fact the microscopic origin of linewidth $(1/T_2)$ is still very far from being fully understood.

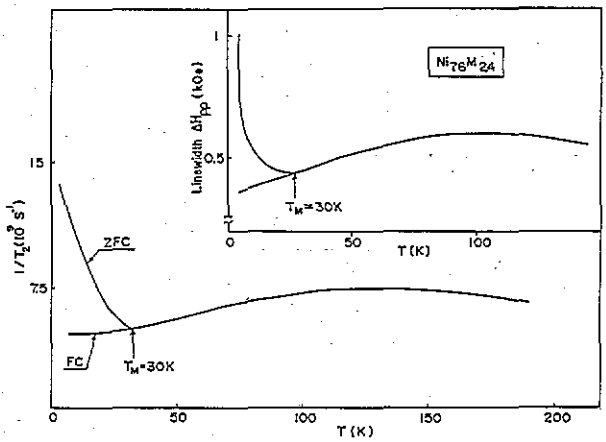

Figure 7. Temperature variation of the resonance linewidth $(1/T_2)$ for both ZFC and FC cases. Inset shows the peak-to-peak linewidth (ΔH_{pp}) as a function of temperature obtained from FMR data.

The temperature dependence of the stiffness constant evaluated using the above model is presented in figure 8. The main qualitative features of this curve are as follows: with decreasing temperature the magnetic stiffness first increases in the superparamagnetic regime then passes through a maximum at the transition temperature ($T_f = 115$ K) from superparamagnetic to spin-glass-like states then decreases smoothly down to $T_M = 30$ K where the unidirectional anisotropy becomes rigid and increases again following the increasing unidirectional anisotropy at lower temperatures. Similar behaviour was observed in $Ni_{79}Mn_{21}$ by neutron diffraction experiments [23]. The magnetic stiffness constant A can be derived from the D value ($A = DM_0/2h$) given as $D_{Ni} = 525$ meV Å^2 and $D_{NiMn} = 85$ meV Å^2 at 4.2 K by Hennion *et al* [23, 25] from an analysis of neutron diffraction experiments. From these values, we obtained $A_{Ni} = 1 \times 10^{-6}$ erg cm^{-1} and $A_{NiMn} = 1 \times 10^{-7}$ erg cm^{-1}, respectively. Our results for $Ni_{76}Mn_{24}$ are between 5.0×10^{-7}–1.5×10^{-7} erg cm^{-1} in the temperature range 4–200 K. The value we obtained is larger than that of Hennion *et al* for NiMn but it is still smaller than that of pure nickel.

The temperature dependence of the anisotropy and resonance fields measured from the intersection of the resonance lines with the baseline are given in figures 9 and 10 respectively. The values of the anisotropies were deduced by fitting the calculated spectra for n-FC and r-FC cases to the corresponding experimental ones. This fitting procedure enabled us to determine H_A and H_K separately. The anisotropy fields were also calculated by using the following expression for the eigenfrequency of the ferromagnetic mode of the system

$$\omega_0 = \gamma[(H_{res} + H_{ani})(H_{res} + H_{ani} + 4\pi M_z)]^{1/2} \qquad H_{ani} = H_K \mp H_A \quad (12)$$

for the case of the parallel geometry. The sign + (−) corresponds to n-FC (r-FC) case. The dashed line in figure 9 corresponds to the values calculated from the fitting and the

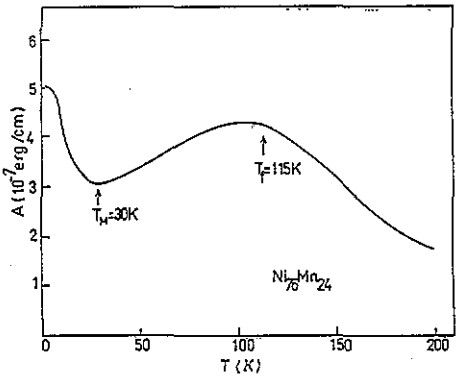

Figure 8. Temperature dependence of the stiffness constant A.

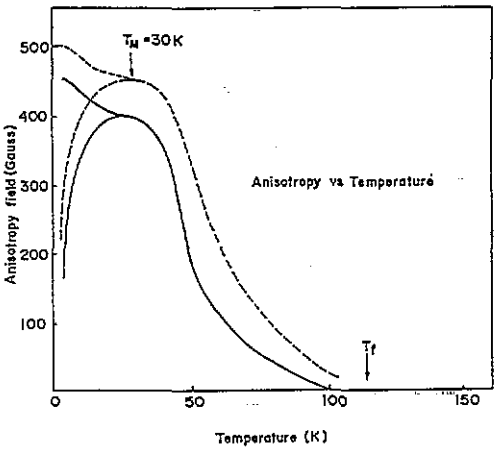

Figure 9. Temperature dependence of the field-induced total anisotropy field ($H_K + H_A$) and H_K deduced from both the fitting (continuous line) and using field values for resonance from figure 10(a) in equation (12).

continuous line corresponds to those obtained by using the expression above. The lower branches at low temperatures belong to H_K, the upper one to the total macroscopic anisotropy ($H_A + H_K$). The anisotropy curves obtained by both methods are qualitatively similar. The total anisotropy first decreases monotonically up to the temperature $T = 30$ K and then decreases more rapidly and vanishes in the temperature range 90–110 K whereas the values of H_K increase first and join the total anisotropy curves at about 30 K where the rigid component of the anisotropy (H_A) vanishes. The differences between the anisotropy values obtained by two different methods is about 50 G below $T = 30$ K, but increases in the temperature range 30–60 K where the A/B ratio (ratio of the lobe amplitude of the resonance line) shows a sharp peak shown in figure 10(b). This implies that the resonance field, H_{res}, is rather difficult to determine accurately from the intersection with the baseline, in view of the broad and asymmetric lineshapes. It should also be noted that the temperature behaviour of the hysteresis losses (figure 3) is very similar to that of H_K (figure 9) determined from FMR, in other words, there is a strong correlation between the dynamic and rigid components of the unidirectional anisotropy H_K and hysteresis effects in NiMn system.

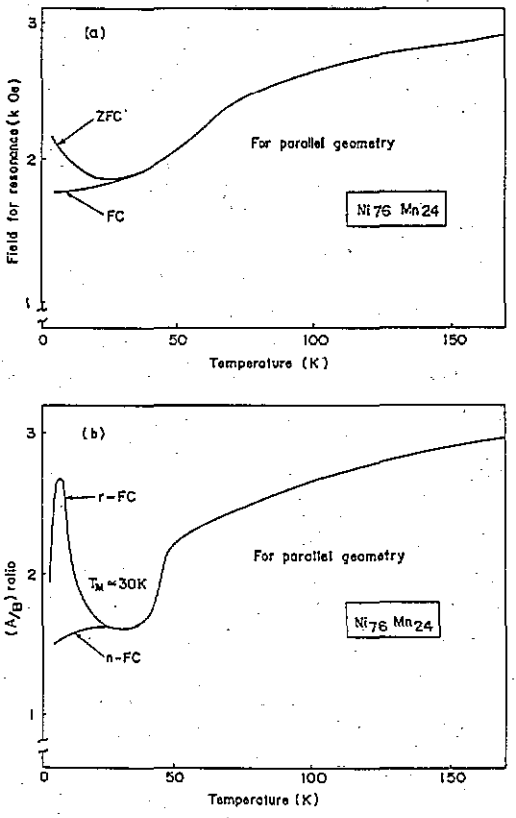

Figure 10. (*a*) Temperature dependence of the resonance fields obtained from the intersection of the base line with the resonance curves. (*b*) The ratio (A/B) of lobe amplitudes of the resonance curves for both *n*-FC (lower branch) and *r*-FC (upper branch) cases. These curves join each other at $T = 30$ K where the rigid component of volume anisotropy vanishes. Note that this ratio for *r*-FC case abruptly increases at about $T = 7$ K, accompanied by a rapid increase of the perpendicular component of surface-induced anisotropy k_2. The rapid rise of the ratio A/B in the temperature range of 30–60 K is also accompanied by a sharp decay of the field-induced volume anisotropy (see figure 9).

As for the surface anisotropy parameters, one can find k_1 and k_2 from ξ_x and ξ_y whose values are indicated in figures 4, 5 and 6. The parameter k_1 (= 0.2 erg cm^{-2} at $T = 4.2$ K) is seen to decrease and then vanish at the temeprature where the unidirectional bulk anisotropy goes to zero, whereas the uniaxial perpendicular component ($k_2 = 0.07$ erg cm^{-2} at $T = 4.2$ K) of the surface anisotropy first rises abruptly and then continues to increase monotonically with increasing temperature. The latter behaviour is not in line with what would be naturally expected from the temperature variation of an anisotropy of pure magnetocrystalline origin. However, the DM anisotropy effects are also likely to be responsible for a sharp drop observed in k_2 when entering the state in which the unidirectional anisotropy sets in. We speculate that the reconstruction of magnetic structure on the surface due to DM interaction gives also an extra contribution to the uniaxial component of the surface anisotropy. As the linewidth increases with increasing temperature, it becomes difficult to determine precisely the values of k_2 from a fitting.

4. Conclusions

The multi-component absorption line arises from the simultaneous solutions of Maxwell's equations and the Landau–Lifshitz dynamic equation of motion for magnetization with surface anisotropy energy. Due to the real component of spin-wave vectors obtained from (3), the microwave component of magnetization decays upon penetrating the sample surface. The spin-wave mode corresponding to a wavevector with the largest real component are mostly localized at the surface region and called surface modes while the remaining ones are called bulk modes. The torque exerted on surface spins by the applied DC field is counteracted by the surface anisotropy field and therefore surface modes may resonate with the applied microwave field at higher DC field values. Consequently, the surface modes appear on the high-field side of usual bulk mode in FMR spectra. The relative intensity of the surface mode to that of the bulk increases with increasing ϵ^2 which includes A, σ and M_z. The separation of these modes shows a directional character indicating unidirectional surface anisotropy. By analysing the shift and the relative intensities, it has proved to be possible to deduce the magnetic stiffness constant A, the surface anisotropy parameters k_1 and k_2 and the phenomenological damping parameter $(1/T_2)$ as a function of temperature. However, in our case the effective exchange constant seems to be overestimated. However, the merit of the model is that it provides a good qualitative description of the experimental spectra. An increase in A, below the freezing temperature T_f, was also seen by Hennion *et al* [23] in neutron diffraction experiment performed on the reentrant $Ni_{81}Mn_{19}$ alloy and was attributed to the microscopic anisotropy contribution to the exchange constant. This effect is of course expected to be much more pronounced in a more anisotropic $Ni_{76}Mn_{24}$ alloy at the temperatures below T_f. This effect can be speculated as follows: from the Landau–Lifshitz dynamic equation of motion for magnetization [1], one can see that the exchange term including A gives an extra contribution to the free energy. An increase in A makes it harder to excite the spin wave, a gradient of the transverse component of the magnetization. On the other hand, it is well known that an abrupt decrease in AC susceptibility is a result of a freezing of the spin system in the temperature range below T_f. Due to microscopic unidirectional anisotropy in this temperature regime, the system is so rigid magnetically that it needs much more energy to deviate the spins from their equilibrium orientations. This effect reflects itself in FMR results as follows:

(i) the amplitude of the transverse microwave component of magnetization decreases and therefore the FMR signal intensity becomes weaker with decreasing temperature below T_f;

(ii) the gradient of average microwave magnetization is also small, consistent with its amplitude, which means that the apparent exchange constant in the spin-glass regime is larger compared to that in the ferromagnetic regime;

(iii) the linewidth increases because of energy loss of the spin system during the passage through the large number of energy minima arising from exchange anisotropy.

We have also carried out some spin-wave resonance experiments on thin films of $Ni_{77}Mn_{23}$ alloys. Preliminary examination of the data reveals that the exchange constant is quite large. The results of this work will be submitted for publication separately.

In our case, both the surface and bulk anisotropies are mainly of an exchange (DM) type. However, the surface anisotropy may include crystalline anisotropy through k_2 as well. In addition to the dynamic component H_k, the bulk anisotropy also includes rigid components H_A directed along the initial orientation of each individual domain magnetization at lower temperatures. The rigid component manifests itself through hysteresis shifts and resonance

field separation between n-FC and r-FC cases. As can be seen from figure 3, these rigid anisotropy fields orient randomly with each domain magnetization making it difficult to saturate the magnetization in ZFC case. As the temperature increases, the dynamic component of the DM anisotropy increases at the expense of the rigid component and as a result

(i) the hysteresis loop gets broader, sharper and more symmetric with respect to the applied DC field direction;

(ii) the resonance lines get narrower in ZFC case;

(iii) the resonance line separation between n-FC and r-FC cases becomes progressively smaller and then vanishes at T_M.

With further increase in T the dynamic component also decays and at T_g the system enters a ferromagnetic-like state. The temperature behaviour of the rigid component of the bulk anisotropy and surface-induced exchange anisotropy are strongly correlated.

Attempts to fit the data for the perpendicular geometry are complicated by the inhomogeneous broadening due to inhomogeneous demagnetizing fields at poor sample surfaces. As the magnetization decreases, the spurious broadening reduces and therefore the fitting improves as shown in figure 6. We have encountered two possible situations for surface modes: if there are surface spin-wave modes in the field perpendicular to the sample surface, no surface mode exists in the parallel configuration and vice-versa. Our results correspond to the former case which is in good agreement with our theoretical expectations. Finally, to clarify the unidirectional surface anisotropy, we are planning to conduct a study on thick films of the same alloys coated with pure nickel, silver and some spin-glass alloys. We have already made some preliminary work on these samples.

Acknowledgments

This work was supported by the Islamic Development Bank and the Scientific and Technical Research Council of Turkey (TBAG-851). One of us (B Aktas) would like to acknowledge the technical assistance of the Department of Physics at the University of California, San Diego.

References

[1] Oner Y, Aktas B, Apaydin F and Harris E A 1988 *Phys. Rev.* B **37** 5866
[2] Aktas B, Oner Y and Harris E A 1989 *Phys. Rev.* B **39** 528
[3] Senoussi S and Oner Y 1983 *J. Magn. Magn. Mater.* **40** 12
[4] Kouvel J S, Abdul-Razzaq W and Ziq Kh H 1987 *Phys. Rev.* B **35** 1768 and references therein
[5] Oner Y and Aktas B 1990 *Phys. Rev.* B **42** 2425
[6] Sato T 1990 *Phys. Rev.* B **41** 2550
[7] Oner Y, Aktas B and Durusoy Z H 1993 *J. Magn. Magn. Mater.* at press
[8] Abdul-Razzaq W 1990 *J. Appl. Phys.* **67** 4907
[9] Teale R W and Pelegrini F 1986 *J. Phys. F: Met. Phys.* **16** 621
[10] Puszkarski H 1979 *Progr. Surf.* **9** 191 and references therein
[11] Rado G T 1982 *Phys. Rev.* B **26** 295
[12] Rado G T and Zhang L 1986 *Phys. Rev.* B **33** 5080
[13] Hippert F, Alloul H and Fert A 1982 *J. Appl. Phys.* **53** 7702
[14] Alloul H and Hippert F 1983 *J. Magn. Magn. Mater.* **31–4** 1321
[15] Rado G T and Weertman J R 1959 *J. Phys. Chem. Solids* **11** 315
[16] Rado G T 1978 *Phys. Rev.* B **18** 6160

[17] Prejean J, Joliclerc M and Monod P 1980 *J. Physique* **41** 427
[18] Levy M P and Fert A 1981 *Phys. Rev.* B **23** 4667
[19] Oner Y, Elkhatouri D and Senoussi S 1986 *J. Magn. Magn. Mater.* **54–7** 159
[20] Durusoy Z H and Oner Y 1990 *Phys. Rev.* B **42** 6831
[21] Campbell I A, Hurdequint H and Hippert F 1986 *Phys. Rev.* B **33** 3540
[22] Hurdequint H, Kouvel J S and Monod P 1983 *J. Magn. Magn. Mater.* **31–4** 1429
[23] Hennion B, Hennion M, Hipperet F and Murani A P 1984 *J. Phys. F: Met. Phys.* **14** 489
[24] Hurdequint H and Kouvel J S 1986 *J. Magn. Magn. Mater.* 54–7 167
[25] Hennion M, Hennion B, Nauciel-Block M and Riedinger R 1976 *J. Phys. F: Met. Phys.* **6** 303